Available online at www.sciencedirect.com

ScienceDirect

Acta Materialia 75 (2014) 134–146

Acta MATERIALIA

www.elsevier.com/locate/actamat

Quantification and modelling of the microstructure/strength relationship by tailoring the morphological parameters of the T_1 phase in an Al–Cu–Li alloy

Thomas Dorin [a,b], Alexis Deschamps [a,*], Frédéric De Geuser [a], Christophe Sigli [b]

[a] SIMAP, INP Grenoble—CNRS—UJF, BP 75, 38402 St Martin d'Hères Cedex, France
[b] Constellium, Voreppe Research Centre, CS 10027, 38341 Voreppe Cedex, France

Received 27 March 2014; received in revised form 15 April 2014; accepted 19 April 2014
Available online 2 June 2014

Abstract

We present a systematic study of the relationship between precipitate microstructure and resulting yield strength in an Al–Cu–Li alloy. By varying the thermomechanical ageing treatments applied to the AA2198 alloy (pre-deformation, heat treatment temperature and duration), T_1 microstructural parameters (thickness, diameter and volume fraction) are varied over a wide range, and the corresponding yield strength is determined. The resulting database of microstructure–strength relationships is used to establish a strengthening model based on interfacial and stacking fault strengthening. This model successfully describes the strength evolution from under-aged to over-aged conditions without the need for a transition from precipitate shearing to by-passing.

Keywords: Precipitation; Aluminium; Strengthening

1. Introduction

The high specific strength, good damage tolerance and excellent property stability of Al–Cu–Li alloys makes them highly attractive for aerospace applications [1–3]. Recently developed Al–Cu–Li alloys can be found, for instance, under the name AIRWARE® [4]. A complex precipitation sequence that relies heavily on thermomechanical treatment is involved in these alloys [5,6]. Cold working prior to the final ageing treatment has been shown to promote precipitation of the T_1-Al_2LiCu phase at the expense of other phases [7–10]. The T_1 phase is known to provide the highest strength [9,11]; it forms as semicoherent platelets along the $\{111\}_{Al}$ planes and exhibits an hexagonal structure [12,13].

The strengthening response associated with the formation of precipitates in Al alloys has been widely studied in the literature [14–17]. In the case of Al–Cu–Li alloys, the T_1 plates were originally thought to be shear resistant [18] and thus attempts have been made to use modified versions of the Orowan equation for precipitate by-passing [18] to model the yield strength increment associated with the T_1 phase [19,20]. The applicability of these early attempts is, however, questionable as T_1 precipitates have been recognised as being shearable for a wide range of heat treatments [21–24]. An interfacial strengthening model, considering the energy required to create a new precipitate–matrix interface when shearing a T_1 plate, has been developed by Nie and Muddle [25]. This model has been only once compared to a limited set of microstructural data [25]. Therefore there is a shortage of quantitative microstructure data available to critically discuss the applicability of the different strengthening models, as well as their

* Corresponding author. Tel.: +33 4 76 82 66 07; fax: +33 4 76 82 66 44.
E-mail address: alexis.deschamps@grenoble-inp.fr (A. Deschamps).

http://dx.doi.org/10.1016/j.actamat.2014.04.046
1359-6454/

robustness and domain of validity. We present in this paper a systematic study in which a wide range of T_1 microstructures are generated by varying the parameters of the thermomechanical treatment, in order to generate a complete database of microstructure–strength relationships. This database will be used to evaluate and to improve the existing strengthening models.

The existing literature indicates that the choice of thermomechanical treatment parameters has a major effect on the resulting precipitation microstructure in Al–Cu–Li alloys [7–10,26,23,27]. The thermomechanical parameters that strongly influence precipitation are: the pre-age stretch, the heat-treatment temperature and the heat-treatment duration. Varying these parameters is a suitable approach to achieve a large variety of T_1 microstructures and provides a strategy for varying the parameters of the precipitate microstructure independently. The heat-treatment temperature has recently been shown to be a key parameter that controls the activation of the T_1 thickening process [27]. Namely, it was shown that at 155 °C the thickness of T_1 precipitates remains constant for very long ageing times at the minimum value of 1.3 nm, and that when temperature is increased from 155 to 190 °C T_1 thickening is quickly activated. In addition, since T_1 nucleates on dislocations, increasing the level of pre-deformation leads to a greater density of smaller precipitates [9]. The influence of pre-deformation on the competitive precipitation of T_1, θ' and δ' has been addressed by Gable et al. [9]. They revealed that the same strength of 450 MPa could be reached for different pre-deformations (0%, 2%, 4% and 6%) that result in significantly different T_1 microstructures: the mean T_1 diameter was found to range from 40 to 160 nm, highlighting that the relationship between the T_1 morphological parameters and the yield strength is not straightforward. However, in the alloy studied by Gable et al., θ' and δ' were also present in considerable amounts, making the analysis complex. We will show in the present study that with an appropriate choice of alloy composition and thermomechanical treatment, the microstructure becomes dominated by T_1 precipitates only.

We recently developed a method to characterise the T_1 phase quantitatively in terms of morphological parameters and volume fraction [27]. This method first uses small-angle X-ray scattering (SAXS) to measure the mean diameter and thickness of T_1 precipitates. SAXS can be carried out in situ during the heat treatments, giving access to the precipitation kinetics [28]. Secondly, this method uses differential scanning calorimetry (DSC) to measure the volume fraction of T_1 precipitates. It will be applied systematically in the present investigation to record the T_1 microstructures for a wide range of thermomechanical treatments. In parallel, the yield strength will also be measured in all the studied heat-treatment conditions. The resulting microstructure–strength characterisation will be then used to challenge the existing models for platelet strengthening; a modified approach to T_1 strengthening will then be proposed.

2. Materials and methods

The AA2198 alloy, whose composition range is given in Table 1, was provided by the Constellium Voreppe Research Centre, France, as rolled 5 mm thick sheets with a fully unrecrystallized grain structure. The samples were first solution treated and water quenched. Directly after quenching, the samples were pre-deformed to a plastic strain ranging from 0% to 12%. The samples were then naturally aged for 7 days. The artificial ageing treatment was executed in an oil bath, starting with a heating ramp of 20 K h^{-1} to 155 °C, followed by an isotherm at 155 °C or by a duplex ageing treatment for 18 h at 155 °C followed by ageing at 190 °C (temperature reached within ~5 min). The samples were quenched in cold water at different times during the ageing and then analysed. In situ SAXS experiments were performed using exactly the same temperature schedules in a dedicated furnace.

SAXS measurements were carried out on a laboratory rotating anode system (Cu K_α source). Prior to the measurements, the samples were mechanically ground down to ~70 μm and mirror polished. The beam size was ~1 mm^2 and SAXS patterns were recorded every 512 s. The distance between the sample and the two-dimensional CCD detector was 351 mm. SAXS patterns were corrected for flat-field and geometrical distortions, and background noise, and then normalised using a glassy carbon as secondary absolute calibration sample [29].

DSC measurements were carried out in a Perkin Elmer Pyris Diamond apparatus. The experiments were conducted under a high-purity nitrogen flux. The heating ramp rate was 50 K min^{-1} from −40 to 520 °C. We chose to start at an initial temperature of −40 °C in order to allow enough time for the apparatus to stabilize when reaching room temperature. The samples consisted of 0.5 mm thick discs 4 mm in diameter in order to fit in the dedicated pure aluminium crucibles. Prior to each DSC measurement, the sample weight was systematically measured for normalisation (range of sample weights: 50–100 mg).

Tensile measurements were carried out using a screw-driven Instron machine with a 30 kN load cell. Special tensile samples with a section gradient were used for preliminary experiments (more details will be given in Section 3.1). Classical tensile samples, with a cross-section of 3 mm × 5 mm and a gauge length of 60 mm, were also used. The extensometer gauge length was 10 mm and the strain rate was 10^{-3} s^{-1}.

Table 1
Composition of AA2198 alloy (wt.%).

AA2198	Cu	Li	Mg	Ag	Zr	Al
Min	2.9	0.8	0.25	0.1	0.04	bal
Max	3.5	1.1	0.8	0.5	0.18	bal

3. Experimental results

3.1. Preliminary study: impact of pre-deformation on hardness

Because T_1 nucleates on dislocations, it is well established that pre-deformation prior to ageing greatly enhances T_1 precipitation kinetics at the expense of other phases such as θ′ or S. The impact of pre-deformation on competitive precipitation and the resulting strength increment has been already reported [7–10]. Pre-deformation directly influences the dislocation density and thus is expected to determine the final T_1 number density, even though some dislocation recovery may take place during sample heating to 155 °C prior to T_1 nucleation. In order to explore the role of pre-deformation in a continuous way and select pre-deformation values that result in significantly different precipitation kinetics, we designed tensile samples of variable section (see Fig. 1(a)) that provide a deformation gradient along the sample during uniaxial stretching. This deformation gradient was characterised accurately using digital image correlation (DIC) [30]. The mean plastic strain along the sample was calculated from the deformation map and plotted as a function of position on the sample (see Fig. 1(b)). In order to cover the entire pre-deformation range with enough precision, we chose appropriate section gradients and used three individual samples. The three samples were subjected to a common ageing treatment, consisting of a 7 day natural ageing at room temperature followed by artificial ageing for 18 h at 155 °C. The impact of pre-deformation on strengthening was evaluated through a series of hardness measurements along the three aged samples (Fig. 1(c)). For this particular ageing time, the results show a continuous increase in strength as a function of pre-deformation, so that changing this parameter can effectively control the precipitation kinetics. For the purpose of our study, we needed additionally to restrict the range of pre-deformations to values where the T_1 phase dominates the microstructure. The distribution of precipitates has been evaluated by ex situ SAXS measurements (see Fig. 2). These measurements make it possible to separate the presence of T_1, θ′ and S phases [28]. The presence of the θ′ and S phases appears to be significant only in the non-pre-deformed sample (Fig. 2(a)), so that a small level of pre-deformation is revealed to be a necessary and sufficient condition for T_1 to dominate the precipitate microstructure in AA2198. The microstructure after ageing of all pre-deformed samples is qualitatively similar irrespective of the amount of pre-deformation (Fig. 2(b)–(d)). Considering the influence of pre-deformation on hardness after ageing, we chose pre-deformations of 0.5%, 2.5% and 12% for further study of precipitation kinetics and related strengthening.

3.2. Microstructure and strength evolution during ageing at constant T_1 thickness

In this section the precipitation kinetics and related strengthening during ageing at 155 °C will be presented for the three selected levels of pre-deformation, namely 0.5%, 2.5% and 12%. The T_1 precipitation kinetics was followed in situ by SAXS for these three conditions. Snapshots of the continuous recording of SAXS images are shown in Fig. 3 for the three deformation levels and selected ageing times. Clearly, increasing the level of pre-deformation results in faster precipitation kinetics, both in terms of the appearance of characteristic streaks for platelet precipitates and subsequent increase of SAXS intensity. Following the method developed by De Geuser et al. [28], the mean diameter and thickness of the T_1 precipitates were extracted from the SAXS images and are plotted in Fig. 4. As expected, a higher pre-deformation (and therefore a higher density of nucleation sites) results in a faster kinetics and smaller mean T_1 diameter at the

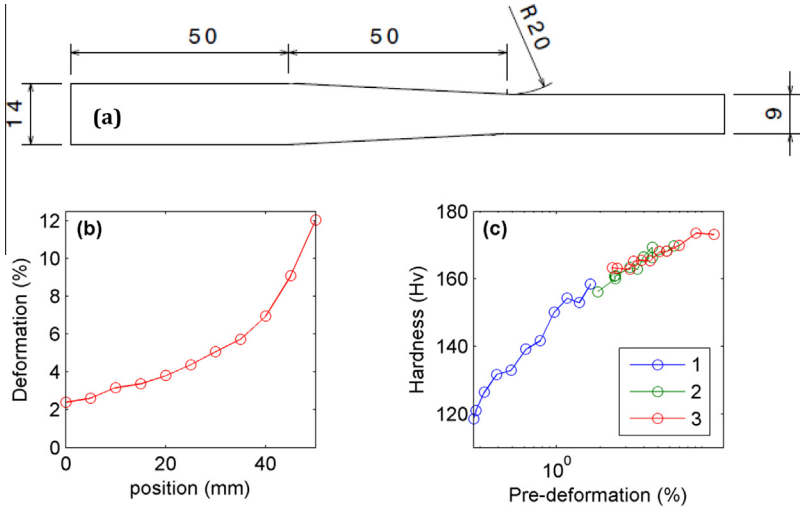

Fig. 1. (a) Uniaxial tensile sample with a section gradient, (b) mean deformation as a function of position along one gradient sample, and (c) hardness measurements plotted as a function of pre-deformation for the three pre-deformed samples covering the complete pre-deformation range and heat treated 18 h at 155 °C.

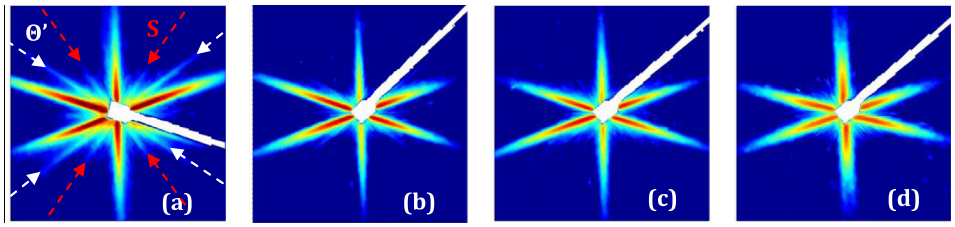

Fig. 2. SAXS images recorded on four samples heat treated for 18 h at 155 °C. The pre-deformations applied prior to the heat treatment were respectively (a) 0%, (b) 0.5%, (c) 2.5%, and (d) 12%.

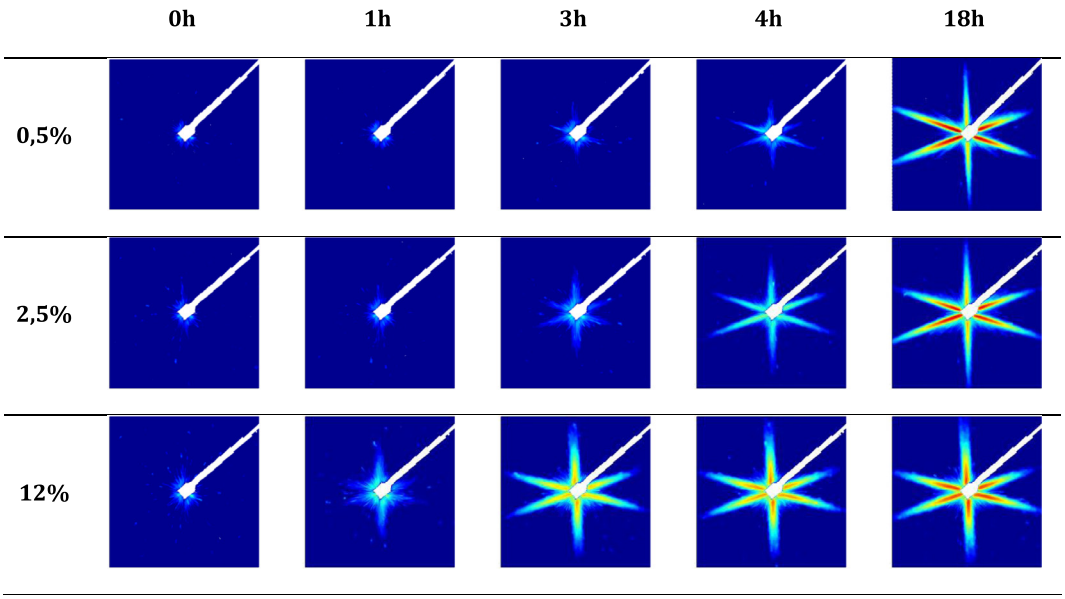

Fig. 3. SAXS images recorded at various times during in situ heat treatment at 155 °C for three different pre-deformations: 0.5%, 2.5% and 12%.

end of the heat treatment. Additionally, one can notice that the mean T_1 thickness remains highly stable around 1.3 nm in the three conditions, which reveals precipitation of only single-layer T_1 precipitates [27]. Fig. 4(c) displays the evolution of T_1 volume fraction extracted from DSC thermograms following the method detailed in Ref. [27]. Finally, information on the diameter, thickness and volume fraction makes it possible to evaluate the number density N of precipitates per unit volume, which is approximated by:

$$N = \frac{4f_v}{\pi t D^2}, \quad (1)$$

where t and D are the T_1 mean thickness and diameter and f_v is the volume fraction of T_1 precipitates (the fitted function shown in Fig. 4(c) is used to estimate the volume fraction at each ageing time). For selected ageing times where the full distribution of plate diameters was available from TEM observations [27], we checked that using the average value of D in Eq. (1) only resulted in a small relative error (not more than 10%.) Fig. 4(a)–(d) emphasise that a stable microstructure is reached in all the conditions after ~150 h at 155 °C. The three resulting microstructures differ in precipitate number density by almost an order of magnitude, and thus in mean T_1 diameter, while keeping a constant T_1 thickness and similar volume fraction. Note that later in this paper, when comparing the yield strength with this microstructure data, the latter will be slightly extrapolated to allow comparison until the last yield strength measurement, namely at 250 h of ageing.

The evolution of yield strength during ageing for the three levels of pre-deformation is shown in Fig. 5 for the same ageing times as those chosen for the measurements of volume fraction. The continuous curves are JMAK-type [31] mathematical functions fitted to the data. This data interpolation will be used in the modelling section to access the yield strength for all ageing times for which microstructural data is available. One can notice that a similar yield strength is reached at the end of the heat treatment for the three conditions. The volume fraction and yield strength evolutions during the heat treatment were found to be very similar in the investigated conditions and within experimental uncertainty a linear relationship is observed between these two parameters (see Fig. 5(b)).

3.3. Microstructure and strength during ageing with evolution of T_1 thickness

In a previous study, we showed that T_1 precipitation occurs in two steps corresponding to two distinct diffusion stages [27], corresponding for the first stage in a precipitate

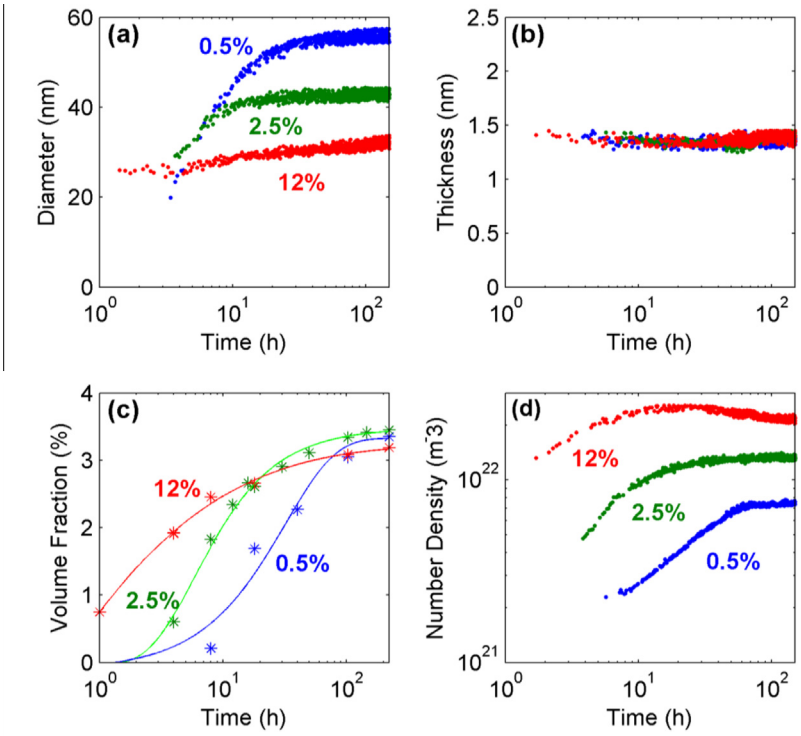

Fig. 4. Evolution of the mean T_1 (a) diameter and (b) thickness extracted from images recorded in situ in SAXS for three pre-deformations (0.5%, 2.5% and 12%). (c) T_1 volume fraction evolution extracted from DSC measurements (absolute uncertainty ±0.1%), and (d) T_1 number density evolution re-calculated from data of (a)–(c).

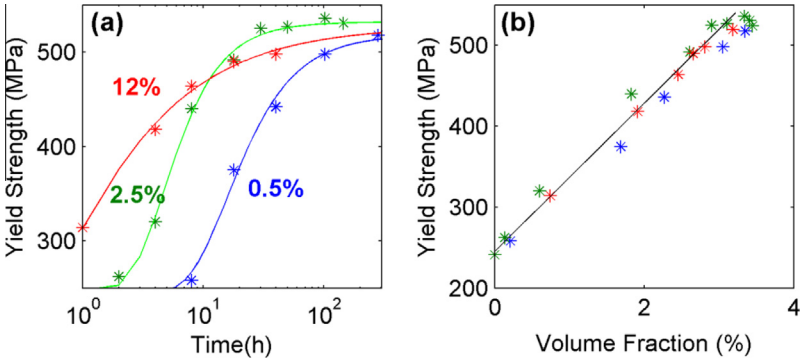

Fig. 5. (a) Yield strength evolution as a function of ageing time at 155 °C and (b) yield strength evolution (absolute uncertainty ±10 MPa) as a function of T_1 volume fraction for the same heat treatments and for the three pre-deformations: 0.5%, 2.5% and 12%.

growth at constant thickness and for the second stage in an increase of precipitate thickness by a ledge mechanism. The use of a duplex ageing treatment at 155 °C followed by 190 °C has proved to be efficient in successively activating these two diffusion stages. In this section, we compare the precipitate microstructures during duplex ageing to the formerly presented single isothermal treatment starting from a sample pre-deformed 2.5%. Fig. 6 shows snapshots of the recorded SAXS images during the two ageing treatments. A significant shortening of the characteristic streaks for the platelet precipitates is observed during ageing at 190 °C (contrarily to 155 °C), which can be related to the increase in precipitate thickness. This qualitative view is confirmed by the quantitative evaluation of the SAXS data. The mean T_1 thickness experiences a significant increase from 1.3 to 2 nm at 190 °C while the mean diameter increases from 40 to 55 nm (Fig. 7(a) and (b)). The volume fraction evolutions, as extracted from DSC measurements, are displayed in Fig. 7(c). A significant increase in volume fraction occurs when temperature is increased to 190 °C but it should be noted that the heat treatment at 155 °C eventually reaches a similar volume fraction after sufficiently long ageing times. The T_1 number density evolutions are evaluated and plotted in Fig. 7(d). The increase

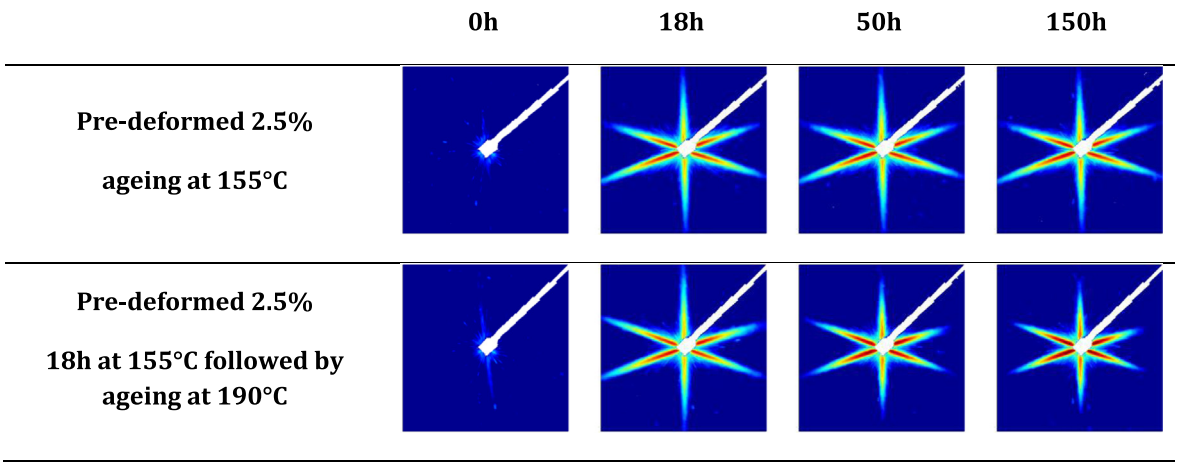

Fig. 6. SAXS images recorded in situ from a sample pre-deformed 2.5%: (a) at 155 °C and (b) 18 h at 155 °C and then at 190 °C, showing in the latter case a shortening of the streaks representative of the thickness increase of the T_1 precipitates at this temperature.

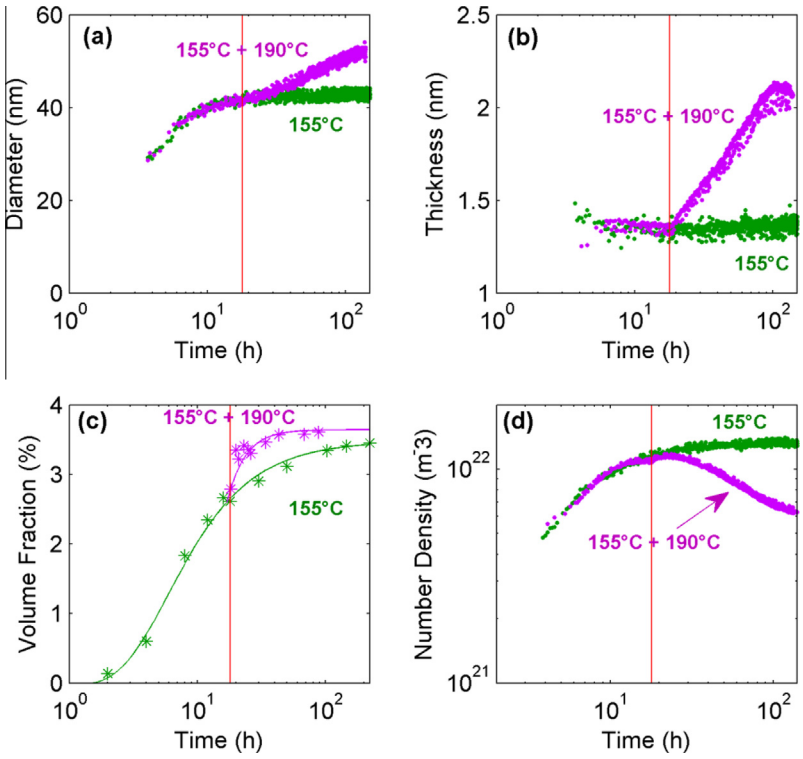

Fig. 7. Evolution of the T_1 precipitate characteristics during ageing of the 2.5% pre-deformed sample at 155 °C (green symbols) and duplex ageing 18 h at 155 °C followed by ageing at 190 °C (purple symbols): (a) T_1 mean diameter and (b) thickness, (c) T_1 volume fraction evolution and (d) T_1 number density. (For interpretation of the references to colour in this figure legend, the reader is referred to the web version of this article.)

in both the thickness and the diameter at 190 °C results in a significant drop of precipitate number density despite the increase in volume fraction.

Fig. 8(a) shows the evolution of yield strength during the duplex ageing treatment at 155 and 190 °C. At 190 °C, the strength first slightly increases in the first few hours and then significantly drops. At the end of the heat treatment the strength has decreased from the peak strength of more than 500 MPa to ~350 MPa. This result highlights the fact that the precipitate thickness seems to play a prominent role in the strength of T_1-containing alloys. Fig. 8(b) shows the yield strength represented as a function of the T_1 volume fraction along the duplex ageing treatment. The monotonous linear relationship between yield strength and precipitate volume fraction that was observed in the case of a distribution of single-layer precipitates no longer applies when the T_1 thickness starts to increase.

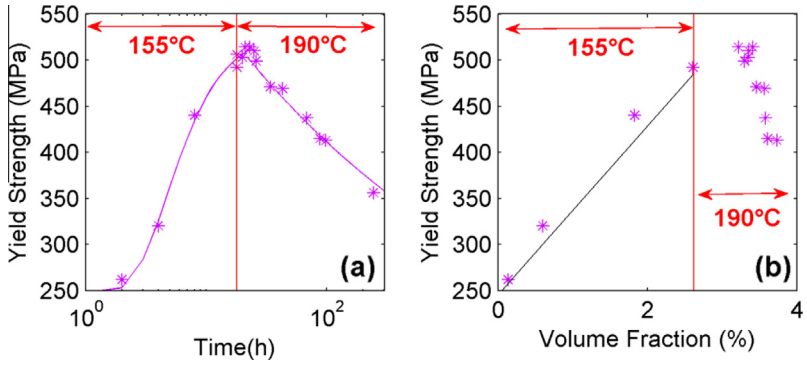

Fig. 8. (a) Yield strength plotted as a function of ageing time and (b) yield strength evolution as a function of T_1 volume fraction during a duplex ageing treatment for 18 h at 155 °C and then at 190 °C from a sample pre-deformed 2.5%.

3.4. Summary of the experimental results

Challenging efficiently the strengthening models to assess their robustness, validity domain and limitations requires obtaining microstructure–strength characterisation for as wide a range of microstructural conditions as possible. Platelet precipitates such as the T_1 phase are characterised by three independent parameters out of the four presented here (thickness, diameter, number density and volume fraction). Our study aims at covering wide ranges of variations of all of these parameters, in order to determine as independently as possible the effect of each of them on the alloy's strength. The range of precipitate microstructures obtained is summarised for all investigated conditions in Fig. 9. We can see that precipitate number densities cover a range of nearly two orders of magnitude. Precipitate diameters range between 20 and 55 nm, and volume fraction between 0.3 and 3.5%. At constant volume fraction, microstructures with a 2-fold difference in precipitate diameter have been generated. At constant diameter, microstructures with a 3-fold difference in volume fraction have been characterised. In addition, the thickness of precipitates has been varied by almost a factor of 2 while keeping a comparable precipitate diameter and volume fraction. This experimental database will now be used to test the ability of the existing yield strength models to predict the yield strength evolutions.

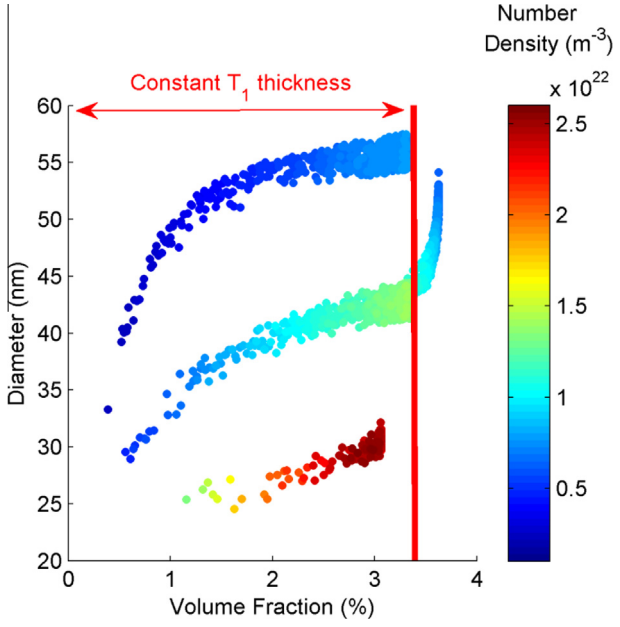

Fig. 9. Map of the T_1 microstructure domain that was explored during the present investigation.

4. Yield strength modelling

4.1. Precipitate–dislocation interaction mechanism

Before attempting to apply existing precipitation strengthening models to our set of microstructural data, it is useful to discuss more in detail the nature of the interaction between the T_1 precipitates and the matrix dislocations. As stated in the Introduction, a number of observations of sheared T_1 precipitates by high-resolution electron microscopy have been published [21–24]. These observations correspond to different alloys and different heat treatments, but in Ref. [24] precipitates were quite similar to those in the present case, namely formed at 155 °C after an applied pre-deformation, and mostly one unit cell thick. The applied strain before observation of these shearing steps was moderate (2% plastic strain), so that the observed mechanism was likely to be representative of that prevailing at the yield point of the alloy. However, it is very difficult to ascertain if the initial interaction mechanism between the dislocations and the precipitate is really shearing, as an alternative would be precipitate bypassing followed by collapse of the Orowan loop and secondary precipitate shearing. Perhaps a good indication (though not a proof) of the fact that precipitates are directly sheared is the absence of strong strain hardening at low strains when thin T_1 precipitates are present in the microstructure [24]. A more detailed study of this question is the subject of an other paper [32]. Therefore, for the

present evaluation we will consider it highly likely that the T_1 precipitates are sheared by the dislocations, but for the sake of completeness we will also evaluate the applicability of the models considering the by-passing of platelet precipitates.

4.2. Models based on the Orowan by-passing mechanism

Modified versions of the Orowan equation have been proposed in the literature to describe the strengthening associated with the presence of semicoherent anisotropic plate-like precipitates. Based on geometrical considerations, the following modified Orowan equation has been suggested by Nie et al. [19] for Al-containing precipitate plates lying on {111} matrix planes:

$$\Delta\tau = 2\frac{Gb}{4\pi\sqrt{1-v}} \times \frac{1}{0.931\sqrt{\frac{0.265\pi Dt}{f_v}-\frac{\pi D}{8}}-0.919t} ln\left(\frac{1.061t}{b}\right), \quad (2)$$

Where $\Delta\tau$ is the critical resolved shear stress (CRSS) increment, $v = 0.36$ is the Poisson's ratio for Al, b is the Burgers vector and G is the shear modulus.

In an alternative study, Zhu and Starke [20] proposed another modified Orowan equation by using computer simulations to examine the dislocation slip process in a random distribution of rectangular obstacles. As a result of these simulations, they proposed the following expression for the CRSS increment of plate-like precipitates lying on {111} matrix planes:

$$\Delta\tau = 0.12G \times \frac{b}{\sqrt{Dt}}\left(\sqrt{f_v}+0.7\sqrt{\frac{D}{t}}f_v+0.12\frac{D}{t}f_v^{\frac{3}{2}}\right)\ln\left(\frac{0.079D}{b}\right). \quad (3)$$

We will test the ability of these two models to predict the yield strength evolutions during the duplex ageing treatment at 155 and 190 °C (described in Section 3.3). In order to convert the CRSS increment into yield strength, the following expression is usually applied:

$$\Delta\sigma = M\Delta\tau + \sigma_0, \quad (4)$$

where M∼3 is the Taylor factor [33], σ_0 is the strength factor including all the other contributions to strengthening (Peierls stress, grain and sub-grain strengthening, solute and dislocation strengthening). For the 2.5% pre-deformed sample, we will approximate σ_0 as the yield strength of a sample at the end of the ramp (free from precipitates), which is ∼250 MPa. Fig. 10 displays the predicted and measured yield strength evolutions. The predictions from these two Orowan-based models are not satisfying as such, particularly in their ability to describe the strengthening around the peak strength. Their prediction could certainly be improved in different ways, such as by changing some parameters (e.g. in the log term of Eq. (3), describing some cut-off distance) or by considering the effect of the inhomogeneous distribution of precipitates in the slip plane and the distribution of plate diameters, similarly to what has been achieved in Al–Cu alloys for θ′ platelets [15]. However, given the evidence for precipitate shearing in this system, we have chosen to concentrate in the following on applying models considering this mechanism.

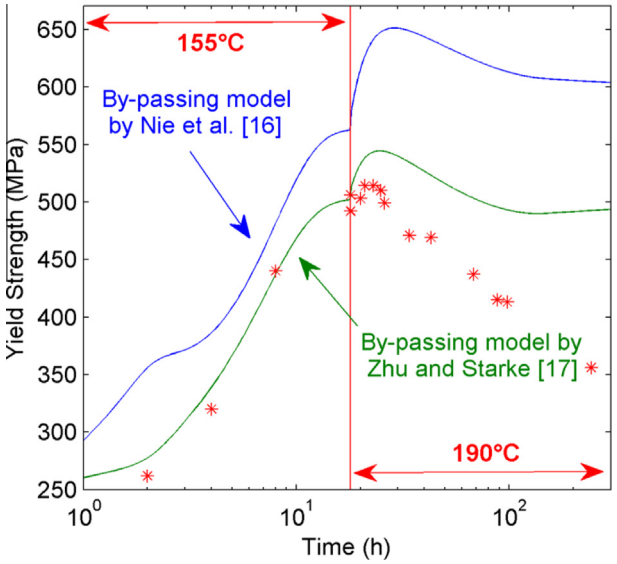

Fig. 10. Experimentally measured yield strength during the duplex ageing treatment (symbols), and predictions by the two models based on the by-passing mechanism (lines).

4.3. Models based on the shearing mechanism

In the following, we will consider models based on the shearing mechanism of the T_1 phase. Shearing a T_1 leads to the creation of a new precipitate–matrix interface and of a stacking fault (SF) as depicted in Fig. 11. Nie and Muddle [25] proposed a model describing the effect of the creation of a precipitate–matrix interface on strengthening. They established the following expression for interfacial strengthening of Al alloys containing regular triangular arrays of shearable $\{111\}_{Al}$ plates:

$$\Delta\tau = \frac{1.211D\gamma_i^{3/2}}{t^2}\sqrt{\frac{bf_v}{\Gamma}}, \quad (5)$$

where γ_i is the precipitate–matrix interfacial energy. However, this model does not include the influence of the formation of a SF on the slip plane within the precipitate, which should be considered when regarding the T_1 shearing process (Fig. 11). Thus we propose a modified version of Nie and Muddle's interfacial strengthening model in order to consider both the new interface and SF contributions to strengthening. Since the details of the derivation of Nie and Muddle's model are not provided in their reference, for the purpose of establishing the modified model we will propose a detailed derivation, which will be shown to result in the same strengthening equation.

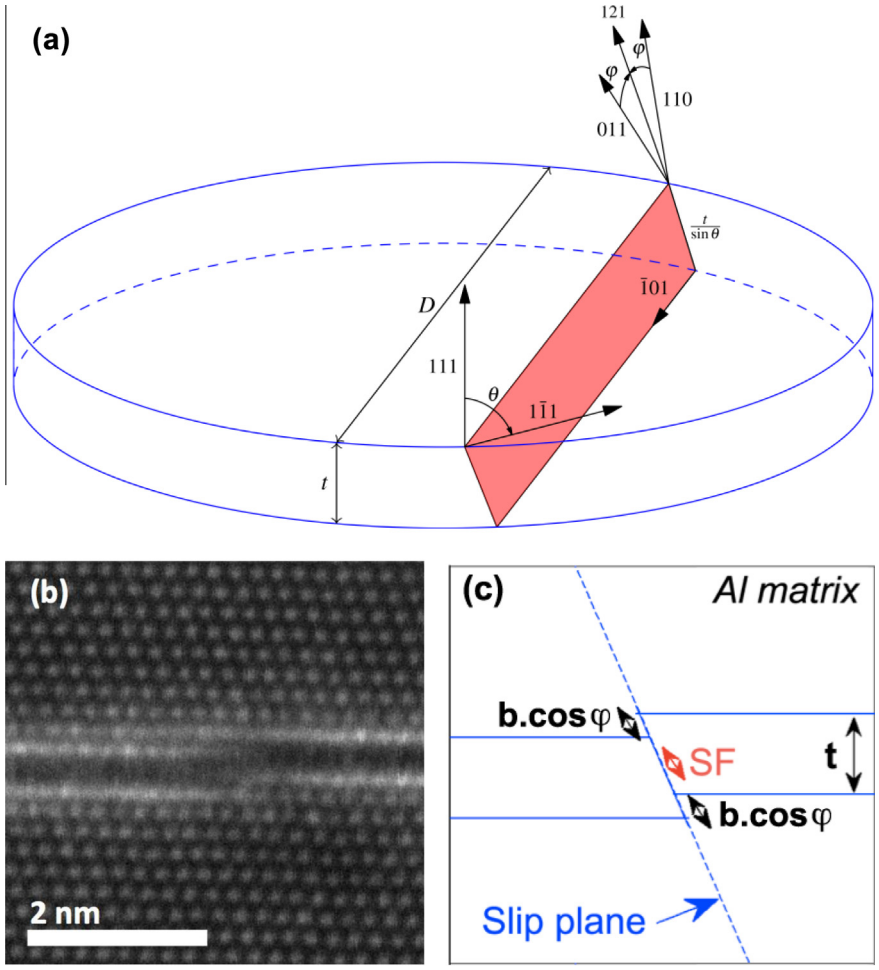

Fig. 11. (a) Scheme of a disc-shaped T1 plate and the trace of the matrix glide plane within the precipitate. The ⟨110⟩ directions possible for the matrix Burgers vector are indicated, as well as the angles used in the model (see text). (b) Image of a sheared T_1 taken in HAADF-STEM along a ⟨110⟩ zone axis. (c) Relationship between the observed step size on this image and the geometrical parameters of (a).

In the approximation of weak obstacles (Friedel statistics), the contribution of shearable precipitates to the strength increment has been described by Guyot [34] as:

$$\Delta\tau = \alpha^{3/2}\left(\frac{\Gamma}{\sqrt{2}bL}\right). \tag{6}$$

where $\alpha = F/\Gamma$ is a parameter that characterises the precipitate's resistance to dislocation glide ($0 < \alpha \leqslant 2$), F is the precipitate strength and Γ is the dislocation line tension in the Al matrix which is approximated as $\frac{1}{2}Gb^2$ where G is the shear modulus, and L is the distance between obstacles in the glide plane. A similar equation can be found in the review by Ardell [35].

Defining the obstacle strength in the case of shearable particles is delicate as many contributions are often involved in the particle shearing mechanism. For the sake of simplicity, we will approximate the T_1 plates to flat cylinders of diameter D and thickness t (Fig. 11(a)). Considering explicitly the distribution of the length of shearing events of these cylinders results in the average shearing diameter of the plate $\widetilde{D} = \pi D/4$. The T_1 shearing mechanism has been recently revealed to only occur by single-steps [24] (Fig. 11(b)). The step length is the intersection of the plate habit plane and the shear plane of the matrix, and therefore is a ⟨110⟩ direction in the Al matrix indices. The width of the step must be measured normal to this direction (therefore in a ⟨112⟩ direction within the glide plane) and therefore it is the projection on this ⟨112⟩ direction of the Burgers vector $b{\sim}0.286nm$, namely b cosφ where $\varphi = 30°$ is the angle between the Burgers vector and the ⟨112⟩ direction.

Thus the area of the new matrix–precipitate interface is $A_i = 2b\widetilde{D}\cos\varphi$ and the area of the SF is $A_{SF} = \widetilde{D}$ (t/sinθ-b·cosφ), where $\theta = 70.53°$ is the angle between two $\{111\}_{Al}$ planes. The energies related to the formation of these new interfaces are:

$$E_i = A_i\gamma_i = 2b\widetilde{D}\cos\varphi\gamma_i, \tag{7}$$
$$E_{SF} = A_{SF}\gamma_{SF} = \widetilde{D}(t/\sin\theta - b\cos\varphi)\gamma_{SF},$$

where γ_{SF} is the interfacial energy corresponding to the created SF.

The strength of a shearable precipitate plate F can be written as the ratio between the energy required to shear

the precipitate and the distance travelled during the shearing event:

$$F = F_i + F_{SF} = \frac{E_i + E_{SF}}{t/\sin\theta} = \frac{2\cos\varphi\sin\theta b\widetilde{D}}{t}\left(\gamma_i + \left(\frac{t}{2b\cos\varphi\sin\theta} - \frac{1}{2}\right)\gamma_{SF}\right) = \frac{\pi\cos\varphi\sin\theta bD}{2t}\gamma_{eff}, \quad (8)$$

where $\gamma_{eff} = \gamma_i + \left(\frac{t}{2b\cos\varphi\sin\theta} - \frac{1}{2}\right)\gamma_{SF}$

The mean planar centre-to-centre precipitate spacing L has been expressed by Nie and Muddle [19] considering triangular arrays distribution of $\{111\}_{AL}$ plates:

$$L = 0.931\sqrt{\frac{0.265\pi Dt}{f_v}}. \quad (9)$$

By combining Eqs. (6), (8) and (9), we can deduce the following expression for the CRSS increment attributed to shearable $\{111\}_{Al}$ plate-like precipitates:

$$\Delta\tau_{T1} = \frac{1.211D\gamma_{eff}^{3/2}}{t^2}\sqrt{\frac{bf_v}{\Gamma}}. \quad (10)$$

This expression is a modified version of Eq. (5), which accounts for the creation of both the new interface and the SF. If the SF energy within the precipitate is set to zero, the model is equivalent to Nie and Mude's model.

The yield strength evolutions, as predicted by Eqs. (5) and (10), are plotted together in Fig. 12 for the duplex ageing treatment, where the interfacial energies (only γ_i for the original model, γ_i and γ_{SF} for the modified model) are fitting parameters. The predictions at constant T_1 thickness are necessarily the same for both models because the relative influence of the interfacial energy creation and SF area remain constant in this case. However, one can notice that the predictions differ when the T_1 precipitates are thickening. The contribution of the SF to the yield strength becomes more important for thicker plates, which results in a higher predicted yield strength.

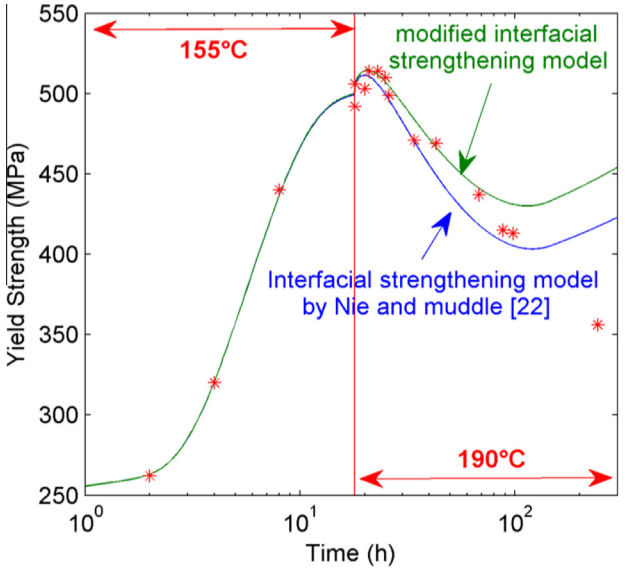

Fig. 12. Experimentally measured yield strength during the duplex ageing treatment (symbols), and predictions by the two models based on the shearing mechanism (lines). The interfacial strengthening by Nie and Muddle corresponds to Eq. (5) and the modified interfacial strengthening curve corresponds to Eq. (10).

In the case of Nie and Muddle's model the fitted interfacial energy is $\gamma_i = 0.107$ J m^{-2}. For the modified interfacial strengthening model, the following interfacial energies are found: $\gamma_i = 0.085$. J m^{-2} and $\gamma_{SF} = 0.005$ J m^{-2}. These energies are in the range of classical interfacial energy values for semicoherent precipitates. However, one can notice a significant difference between the interfacial and stacking fault energies. The relatively high amount of energy required to create a new interface is related to the difference in precipitate and matrix structures, which results in a high strain field at the new created interface. The presence of this high strain field gives rise to a blurry contrast in HAADF-STEM around the sheared region (see Fig. 11(b)). For the Ω phase in Al alloys, Li and Wawner [36] revealed that the interfacial energy for the new interface increases dramatically with multiple shearing events, which makes multiple shearing highly unfavourable, as confirmed recently for the T_1 phase by the observations of Deschamps et al. [24]. On the other hand, the creation of a SF, which is internal to the precipitate may result in a smaller energy increase, especially if an atomic rearrangement follows the shearing event. Since the main energy contribution is that of the interfacial step, a natural outcome is that Nie and Muddle's interfacial strengthening model is able to predict accurately the yield strength evolution by only considering the creation of the new precipitate–matrix interface while neglecting the SF creation. However, the modified interfacial strengthening model should be physically more correct and even though it brings only a marginal benefit in terms of the description of experimental data, we will thus use it in the following.

One important observation resulting from the fit of the model to the experimental data is that it describes very accurately the first stages of the ageing treatment at 190 °C, where all parameters (namely diameter, volume fraction and thickness) vary very quickly. At peak strength, the average obstacle strength can be calculated from the model (Eq. (8)), in order to estimate the value of parameter α in Eq. (6). The result is $\alpha = 0.7$, much lower than the value of 2 for non-shearable precipitates, which indirectly validates the hypothesis that precipitates are sheared by dislocations. The model is also capable of describing a large part of the strength decrease during over-ageing at 190 °C, confirming that it is not necessary to invoke a precipitate by-passing mechanism even at these relatively late stages of ageing. In fact, T_1 precipitates thicker than one unit cell have been observed to be sheared in the literature [22]. At very late ageing times (last point at 250 h of ageing) the model prediction strongly deviates from the experimental data. In particular, an increase of yield strength is predicted, whereas the experimental one is observed to

continuously decrease. This predicted increase is related to the fact that experiments at these long ageing times show a stabilization of the precipitate thickness and a continuous increase of the precipitate diameter. This deviation between the experiments and the model could be related to a change in the precipitate–dislocation interaction mechanism.

4.4. Applicability of the modified interfacial strengthening model to the different T_1 kinetics

The preceding section showed that the modified interfacial strengthening model (Eq. (10)) is suitable to describe the yield strength evolution in the presence of T_1 precipitates. In order to test the robustness of this model, we calculated the yield strength evolutions for the ageing treatments with different pre-deformations studied in Section 3.2, using the measured microstructural parameters for the T_1 precipitates. As shown in Fig. 13, the model can be successfully applied to this data, provided that the base strength in the absence of precipitates σ_0 is adjusted depending on the pre-deformation value. σ_0 was respectively adjusted to 152, 250 and 310 MPa for the 0.5%, 2.5% and 12% pre-deformations. The significance of this adjustment will be discussed in the next section.

5. Discussion

The experimental database of microstructure–strength relationships that we generated makes it possible to test the capability of precipitation strengthening models to describe the effect of precipitation of T_1 on yield strength. We have shown that models based on the by-passing mechanism were unsuccessful in describing our experimental results, which is consistent with the now widely accepted shearable nature of the T_1 precipitates. On the other hand, Nie and Muddle's model for interfacial strengthening by platelet precipitates [25] has been shown to provide a good agreement with the experimental data. A modified version of this model has been shown to successfully describe a wide range of experimental data, including the transition on each side of the peak-aged state. This agreement strongly suggests that the peak-ageing state is not related in this case to a change of precipitate-dislocation mechanism from precipitate shearing to precipitate by-passing as is commonly observed in some Al alloys such as Al–Zn–Mg–Cu alloys [37,38]. Instead, the experimental data and the model agree in attributing the strength decrease after peak ageing to an increase in precipitate thickness ($\Delta\tau \propto t^{-2}$), consistently with the prominent role played by the creation of steps at the precipitate–matrix interfaces during the shearing process. However, for very long over-ageing the model predictions deviate strongly from the experimental data, suggesting a change in strengthening mechanism. When T_1 precipitates reach a sufficient thickness and when their number density becomes sufficiently small so that their spacing increases, it seems reasonable that the by-passing mechanism should be activated. However, it can be noted that the models based on the

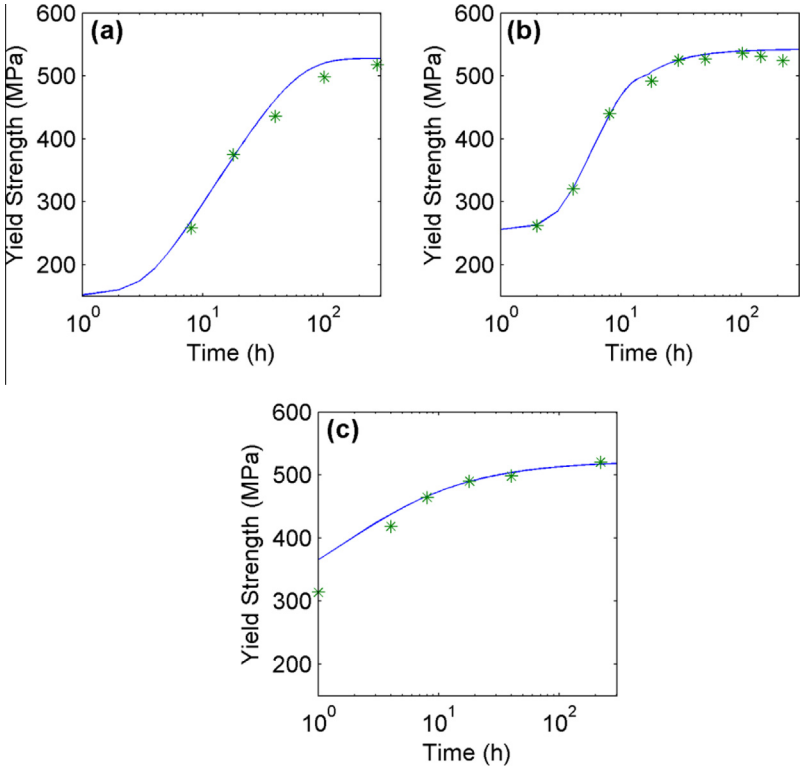

Fig. 13. Experimental yield strength measurements (symbols) and evolutions as predicted from Eq. (10) (lines) as a function of ageing time during a heat treatment at 155 °C and different pre-deformations: (a) 0.5%, (b) 2.5%, and (c) 12%.

by-passing mechanism do not predict the good range of strengthening for these overaged conditions either. The influence of precipitate microstructures on this possible change in strengthening mechanism requires a more detailed study of the alloy's plasticity that will be reported in a separate paper [32].

The modified interfacial strengthening model has been shown to be applicable to all the investigated thermomechanical treatments, including ageing treatments where the pre-deformation had been varied, resulting in a wide range of precipitate number densities. However, this adjustment required different base strengths σ_0 to be chosen depending on the initial pre-deformation. One possibility is that this difference reflects the influence of pre-deformation on dislocation strengthening. In fact, the flow stress during the tensile test used for stretching is approximately 100, 150 and 300 MPa for, respectively, the 0.5, 2.5 and 12% pre-deformations (part of this flow stress could be recovered during the first stages of ageing). The remaining difference could be due to the presence on the dislocations of other phases such as Mg-rich precipitates that have been shown to form together with the T_1 precipitates [39]. This can explain the relatively high strength of the sample at the end of the heating ramp to 155 °C when no significant T_1 precipitates are present (250 MPa for the 2.5% pre-deformed material).

Assuming that this description of T_1 strengthening is correct, it has a number of interesting consequences. Firstly, it implies that the linear relationship, independent of pre-deformation, that was experimentally observed between yield strength and T_1 precipitate volume fraction (Fig. 5(b)) is not supported by our model. In fact, it results from a compensation of the change in precipitation strengthening by a change in base strength with pre-deformation. Eq. (10) of our model can be written as $\Delta\tau \propto f_v N^{-1/2} t^{-5/2}$, meaning that the linear relationship between volume fraction and strengthening increment holds only for a constant precipitate thickness and number density. The constant precipitate thickness is a valid assumption during ageing at 155 °C (Fig. 4(b)); however, the precipitate density changes moderately during the ageing treatment after a given pre-deformation, and strongly from one pre-deformation to another. This change in precipitate density explains the necessary compensation of a loss of strengthening by an increased base strength to describe the entire range of studied microstructures.

It may seem at first sight counter-intuitive that the precipitate strength should decrease when the precipitate number density becomes higher, at constant volume fraction and thickness. Such a dependence on precipitate number density is opposite to what happens with strengthening by spherical precipitates. However, it can be better understood if Eq. (10) of our model is reorganized in yet another way as $\Delta\tau \propto D^2 N^{1/2} t^{-3/2}$ where the volume fraction does not appear explicitly. This form of the equation shows that both the precipitate number density and precipitate diameter contribute positively to the strengthening increment; however, the diameter makes a much stronger contribution, because increasing the precipitate diameter has a large effect on the precipitate strength. Consequently, increasing the precipitate number density at constant volume fraction and thickness (such as is achieved by increasing the pre-deformation), which necessarily results in a decrease of their diameter, induces a decrease in the precipitate strengthening contribution.

6. Conclusion

(1) By combining the effect of pre-deformation, ageing time and ageing temperature, a wide range of T_1 microstructures have been obtained. The parameters of the T_1 precipitate distributions have been systematically characterised in terms of precipitate thickness, diameter and volume fraction, and the resulting number density has been calculated. The yield strengths corresponding to these microstructures have been systematically measured, resulting in a large database of microstructure–strength relationships.

(2) The yield strength evolution, in the case of strengthening by T_1 precipitates, has been successfully described using a model for precipitate shearing considering the combination of interfacial and stacking fault strengthening. The transition at peak strength and subsequent decrease in yield strength are successfully represented without accounting for a shearing-to-by-passing transition.

(3) The interfacial strengthening model overestimates the yield strength for highly over-aged samples. This result suggests that a transition in strengthening mechanisms occurs in the late stages of precipitation. An alternative model is necessary to predict the yield strength for these conditions.

Acknowledgements

Prof. P. Guyot is warmly thanked for fruitful discussions. Dr. W. Lefebvre is thanked for helping with the STEM-HAADF imaging. The referee is thanked for providing useful comments on the work.

References

[1] Williams J, Starke Jr E. Acta Mater 2003;51:5775–99.
[2] Warner T. Mat Sci Forum 2006;519–521:1271–8.
[3] Rioja R, Liu J. Metall Mater Trans A 2012;43A:3325–37.
[4] Daniélou A, Ronxin J, Nardin C, Ehstrom J. In: Proceedings of the 13th international conference on aluminium alloys. Pittsburgh, PA: TMS, Warrendale, PA; 2012. p. 511–6.
[5] Hardy H, Silcock J. J Inst Met 1955–56;84:423–8.
[6] Sainfort P, Dubost B. J Phys 1987;48:407–13.
[7] Cassada WA, Shiflet G, Starke Jr E. Metall Trans A 1991;22A:299–306.
[8] Ringer S, Muddle B, Polmear I. Metall Mater Trans A 1995;26A:1659–71.

[9] Gable B, Zhu A, Csontos A, Starke EA. J Light Met 2001;1:1–14.
[10] Decreus B. Study of the precipitation in third generation Al-Li-Cu alloys – Relationships between microstructure and mechanical properties [Ph.D. thesis. Grenoble Institute of Technology; 2010.
[11] Decreus B, Deschamps A, De Geuser F, Donnadieu P, Sigli C, Weyland M. Acta Mater 2013;61:2207–18.
[12] Donnadieu P, Shao Y, De Geuser F, Botton G, Lazar S, Cheynet M, et al. Acta Mater 2011;59:462–72.
[13] Dwyer C, Weyland M, Chang L, Muddle B. Appl Phys Lett 2011:98.
[14] Deschamps A, Brechet Y. Acta Mater 1998;47:293–305.
[15] Da Costa Teixeira J, Cram D, Bourgeois L, Bastow T, Hill A, Hutchinson C. Acta Mater 2008;56(120):6109–22.
[16] Myhr O, Grong O, Pedersen K. Metall Mater Trans A 2010;41A:2276–89.
[17] Bardel D, Perez M, Nelias D, Deschamps A, Hutchinson C, Maisonnette D, et al. Acta Mater 2014;62:129–40.
[18] Huang J, Ardell A. J Phys 1987;48:373–83.
[19] Nie J, Muddle B, Polmear I. Trans Tech Publ 1996;217–222:1257–62.
[20] Zhu A, Starke E. Acta Metall 1999;47(11):3262–9.
[21] Howe J, Lee J, Vasudevan A. Metall Trans A 1988;19A:2911–20.
[22] Nie J, Muddle B. Mat Sci Eng 2001:448–51.
[23] Csontos E, Starke A. Int J Plast 2005;21:1097–118.
[24] Deschamps A, Decreus B, De Geuser F, Dorin T, Weyland M. Acta Mater 2013;61(11):4010–21.
[25] Nie J, Muddle B. J Phase Equilib 1998;19(6):543–51.
[26] Csontos A, Starke Jr E. Metall Mater Trans A 2000;31A:1965–76.
[27] Dorin T, De Geuser F, Lefebvre W, Sigli C, Deschamps A. Phil Mag 2014;94(10):1012–30.
[28] De Geuser F, Bley F, Deschamps A. J Appl Cryst 2012;45:1208–18.
[29] Zhang F, Ilavsky J, Long G, Quintana J, Allen A, Jemian P. Metall Mater Trans A 2010;41A:1151–8.
[30] Chu T, Ranson W, Sutton M, Peters W. Exp Mech 1985;25(3):232–44.
[31] Avrami M. J Chem Phys 1939;7:1103–12.
[32] Dorin T, De Geuser F, Lefebvre W, Sigli C, Deschamps A. Mat Sci Eng A 2014;605:119–26.
[33] Tayron W, Crooks R, Domack M, Wagner J. Exp Mech 2010;50:135–43.
[34] Guyot P. Interactions des dislocations avec des impuretés fixes. In: Groh P, Kubin LP, Martin J-L., Editors, Dislocations et déformation plastique, Yravals, summer school Yravals 1979, Les Éditions de physique, les Ulis, France, 1980.
[35] Ardell A. Metall Trans A 1985;16A:2133.
[36] Li B, Wawner F. Acta Mater 1998;46(15):5483–90.
[37] Guyot P, Cottignies L. Acta Mater 1996;44:61–7.
[38] Fribourg G, Bréchet Y, Deschamps A, Simar A. Acta Mater 2011;59:3621–35.
[39] Araullo-Peters V, Gault B, De Geuser F, Deschamps A, Cairney J. Acta Mater 2014;66:199–208.